Journal of Power Sources 202 (2012) 166–174

Contents lists available at SciVerse ScienceDirect

Journal of Power Sources

journal homepage: www.elsevier.com/locate/jpowsour

The investigation of interaction between $La_{0.9}Sr_{0.1}MnO_3$ cathode and metallic interconnect for solid oxide fuel cell at reduced temperature

Juan Wu, Dong Yan, Jian Pu*, Bo Chi, Li Jian

School of Materials Science and Engineering, State Key Laboratory of Material Processing and Die & Mould Technology, Huazhong University of Science & Technology, Wuhan, Hubei 430074, China

ARTICLE INFO

Article history:
Received 24 August 2011
Received in revised form
17 November 2011
Accepted 18 November 2011
Available online 30 November 2011

Keywords:
Solid oxide fuel cell
Cr deposition
Interconnect
Sr-doped lanthanum manganite cathode

ABSTRACT

The Cr deposition reaction is investigated between the $La_{0.9}Sr_{0.1}MnO_3$ (LSM) cathode and Fe–Cr alloy interconnect at 750 °C for solid oxide fuel cell. The poison effect on cathode is observed by a group of orthogonal experiments at the presence of Fe–Cr alloy involving with air flow and current passages. After the current polarization, the cathode layer has been delaminated from the electrolyte (YSZ), and the Cr deposition reaction is accelerated with adding air partial pressure. When the LSM cathode has undergone Cr poison for 3000 min with current passage of 400 mA cm^{-2} and air flow of 100 mL min^{-1}, two rapid increase stages of polarization potential $E_{cathode}$ are found, which can be reasonably explained by Cr deposition resulting in cathode delaminated from the electrolyte layer. Furthermore, the Cr deposition ring and two kinds of Cr-contain agglomerates are observed in the interface of LSM/YSZ, which indicates that the formation of Cr_2O_3 and $(Cr,Mn)_3O_4$ oxides, respectively. This suggests that the deposition of Cr species would preferentially occur at the three phase boundary region and the trend to agglomeration in long time operation.

1. Introduction

Solid oxide fuel cell (SOFC) has been generally defined as a promising alternate energy in worldwide owing to the high energy conversion efficiency and low pollution emission. Because the operation temperature of SOFC has been reduced from 1000 °C to 600–800 °C, some metallic-type interconnects are developed in intermediate-temperature SOFC [1,2]. As a key component in SOFC, the metallic interconnect should provide excellent oxidation resistance and electrical conductivity in the operating atmosphere, and good compatibility with the adjacent components [3–5]. Chromia forming alloys, as the most widely developed material for metallic interconnect in SOFC, have suitable coefficient of thermal expansion (CTE) with other components and acceptable oxidation resistance in high temperature [6–8]. However, using as interconnect, the chromia forming alloys have an essential challenge that the volatile Cr species such as CrO_3 and $Cr(OH)_2O_2$ will generate from chromium oxide scale at high temperature [9–11]. When the gaseous Cr species are deposited on the surface of electrode and interface of cathode/electrolyte, it may cause rapid cell performance degradation. This phenomenon is known as the Cr poisoning of cathode [12–16]. It has been recognized as a critical challenge in degradation of stack performance if chromia forming alloys are recommended as the candidate materials for the interconnect [17–19].

Recent researches have studied the interaction between the cathodes and metallic interconnects closely to make efforts on demonstrating the mechanism and kinetics of Cr poisoning cathode. Jiang has investigated the O_2 reduction reactions on Sr-doped $LaMnO_3$ (LSM) cathodes and TZ3Y electrolyte which suggested that Cr deposition was not originated from electrochemical reduction of gas Cr species, but from a chemical reaction related to the nucleation reaction between the nucleation agent and the gaseous Cr species. Specially, the nucleation agent of the LSM cathode is the Mn species [20]. For (La, Sr)(Co, Fe)O_3 (LSCF) cathodes system, the Cr deposition in the LSCF/GDC system is affected by the Sr species-enriched/segregated [21]. Konycheva et al. had proposed other viewpoints on which indicating the mechanism of the Cr poisoning cathode. They studied the Cr deposition on LSM and LSCF cathodes, and considered that the presence of solid chromium oxide would block the electrochemical active sites, and hence induce the decomposition of the cathode [12].

However, the cation diffusion in the LSM cathode will decrease at the reduce temperature, so the Cr deposition mechanism based on Mn^{2+} migration may not work at lower temperature. In this paper, the phenomenon of Cr poisoning LSM cathode was investigated at 750 °C in the presence of a chromia-forming alloy interconnect, and the mechanism was discussed by evaluating the effect of air flow and current passage.

* Corresponding author. Tel.: +86 27 87558142; fax: +86 27 87558142.
E-mail address: pujian@hust.edu.cn (J. Pu).

0378-7753/$ – see front matter © 2011 Elsevier B.V. All rights reserved.
doi:10.1016/j.jpowsour.2011.11.054

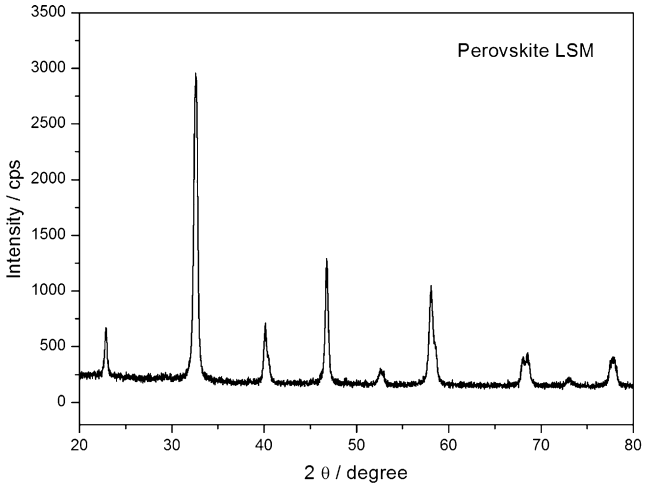

Fig. 1. XRD pattern of LSM powders.

2. Experimental details

2.1. Sample preparation

The Cr-containing 14 wt.% ferritic stainless steel (Yuechang Ltd., China) was chosen as metallic interconnects. The alloy was machined into square coupon (12 mm × 12 mm × 4 mm thick) with channels (1.2 mm × 1.2 mm deep), and small holes were made as air entrances in the middle of each channel.

The $La_{0.9}Sr_{0.1}MnO_3$ (LSM) powder was prepared by citrate-gel method that acid was added as agent with mixing $LaN_3O_9{\cdot}6H_2O$, $Sr(NO_3)_2$ and $Mn(NO_3)_2$ in ethylene glycol. After dried, the gel was grinded and then calcined at 800 °C for 2 h to obtain LSM powder. A PANalytical X'Pert PRO X-ray diffraction (XRD) was used for indentifying phase structure with Cu $K\alpha_1$ radiation ($\lambda = 0.1504$ nm) at room temperature. The XRD pattern of powder has showed a pure perovskite structure in Fig. 1. The LSM cathode paste was applied on YSZ electrolyte substrate by screen printing and then sintered at 1150 °C for 2 h. The thickness of YSZ pellet was about 1 mm with 20 mm in diameter, and the cathode area on the electrolyte was about 0.5 cm^2. The Pt paste (Guiyan Platinum Ltd., China) was painted on the opposite side of the YSZ electrolyte pellet as the counter electrode and reference electrode with a distance of 4 mm between them. In the test system described in Fig. 2, metallic interconnect was set up on the cathode, and a Pt mesh between them was used to collect current. A quartz tube on top of interconnect was severed as air flow path so that air could fill the channel by passing the hole on interconnect. On two sides of interconnect, Pt leads were spot-welded to serve as the voltage and current probes.

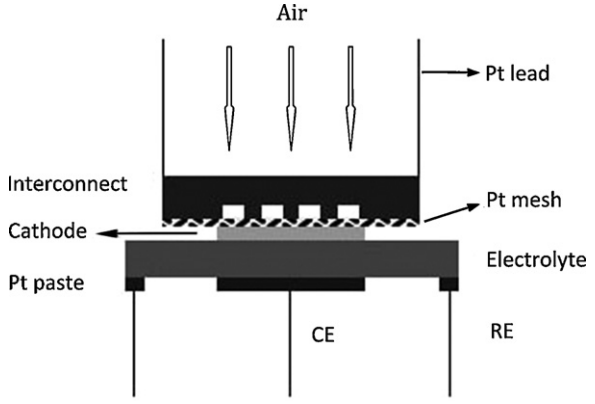

Fig. 2. Arrangement of the test system.

2.2. Electrochemical measurement and characterization

The half-cell/interconnect system was placed in a tube furnace which including the three-electrode and four-wire structure. Pt wires were conducted to collect signal of current and other electrochemical parameters. The sample was investigated by impedance without current and air flow at 750 °C as a referential baseline to compare the effect of the air flow and current passage. A constant current of 400 mA cm^{-2} was loaded to the samples for 1200 min, and the Electrochemical Impedance Spectroscopy (EIS) was applied to measure electrochemical polarization and resistance. The EIS measurement was carried out by a Solartron 1260 frequency response analyzer and a 1287 electrochemical interface in the frequency range of 0.1 Hz to 100 kHz with the amplitude of 10 mV. Electrode ohmic resistance (R_Ω) was measured from the high frequency intercept [22], and the electrode polarization resistance (R_E) was directly obtained from the difference between the high frequency and the low frequency intercepts on the impedance spectra. Furthermore, the overpotential (η) was obtained from $E_{cathode}$ and R_Ω by the following equation [23]:

$$E_{cathode} = \eta + jR_\Omega \quad (1)$$

where j is the current density. The tests with prolonged polarization time 1200 min and 3000 min were respectively studied to demonstrate the relationship between electrochemical parameters and time. The microstructure of the surface and cross-sectional of cathode and electrolyte were characterized by using a FEI Sirion 200 field emission scanning electron microscope (SEM) with energy dissipation spectrum (EDS) attachment.

3. Results and discussion

In order to demonstrate the effect of Cr poisoning between the LSM cathode and the Fe–14Cr% interconnect alloy, a group of orthogonal experiments involving current passage and air flow were designed as shown in Table 1. First of all, we directly perceived the change in EIS without the air flow and current passage. Then, air flow of 100 mL min^{-1} and current passage of 400 mA cm^{-2} were respectively offered to the cathode side to compare the change of EIS parameters. In the end, both of air flow and current passage were introduced to observe Cr deposition and the effect of poisoning cathode.

Fig. 3 shows the impedance of the LSM cathode at 750 °C for 1200 min in the presence of a Fe–Cr alloy. Without an air flow, the polarization resistance (R_E) increased from 28.4 Ω cm^2 to 42.7 Ω cm^2 by amplitude of 50% during the first 240 min, and then maintained basically stable. When the LSM cathode was fed with air flow of 100 mL min^{-1}, the impedance arc became larger, which indicated that the R_E was increased. The R_E increased from 54.7 Ω cm^2 to 60.5 Ω cm^2 by amplitude of 10.6% in the first 240 min which was lower than that without air flow. The R_Ω for both samples have a slight decreasing trend, which is most likely due to improved contact between the cathode and the electrolyte [24]. The

Table 1
The group of orthogonal experiments.

Condition	In open air	With air flow of 100 mL min^{-1}
Without current	①	②
With current of 400 mA cm^{-2}	③	④

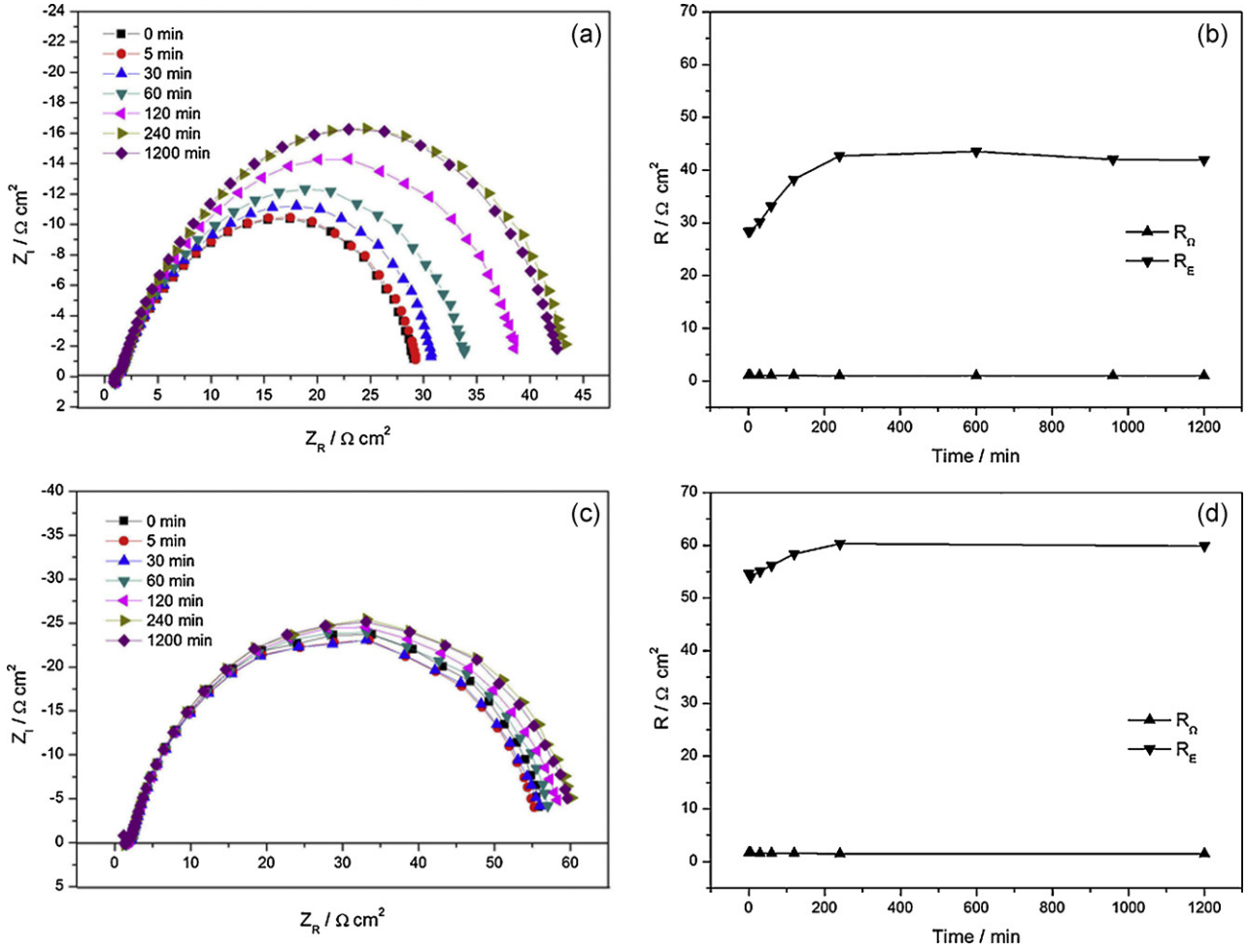

Fig. 3. Initial the impedance and resistance of LSM cathode in the presence of Fe–Cr alloy as a function of time at 750 °C for 1200 min in open air (a and b) and with air flow of 100 mL min^{-1} (c and d).

small changes of the R_E and R_Ω in the long term operation implies that no obvious effect of Cr deposition exists in the situation.

Fig. 4 shows the SEM micrographs of the Cr deposition on different areas of cathode in presence of a Fe–Cr alloy at 750 °C for 1200 min. In the open air, the cathode surface was covered with fine particles, and it was also found on the surface of YSZ near the edge of cathode. The fine particles were too tiny to make certain characterization. According to the further growth of the crystals in the later work of this paper, the deposition particles were likely to be the Cr-rich phase such as Cr_2O_3 as reported [20]. In contrast, the cathode surface was covered with a dense layer of the Cr deposition when with air flow. It could be also seen that large grains on the YSZ electrolyte near the edge of LSM cathode distributed around the surface of electrolyte in the shape of flake-like with size of 1–2 μm. When the LSM cathode particles were removed from the electrolyte, the contact rings with diameter of 1–2 μm on the surface of electrolyte were seen, and an inconspicuous layer of deposit could be confirmed to be Cr-contained oxide phase [25]. The amount of Cr deposition would be significantly increased with air flow added, because the chromium vaporization rate of Cr_2O_3(s) was promoted and then there would be more Cr-contained gaseous species supplied to the cathode [26].

The initial impedance and polarization trends of LSM cathode in the presence of Fe–Cr alloy were different from the long-term polarization with current passage. Fig. 5 shows the initial impedance and polarization responses of LSM cathode under a cathodic current of 400 mA cm^{-2} at 750 °C in open air (Fig. 5(a) and (b)), and in air flow of 100 mL min^{-1} (Fig. 5(c) and (d)) at the presence of Fe–Cr alloy. In contrast with those in the open circuit, the initial impedance was decreased with the current passage due to the presence of Fe–Cr alloy. In open air, the R_E reduced from 78.4 Ω cm^2 to 29.3 Ω cm^2 by 62.6% which was contrary to that without current passage. When the current was loaded on the cathode, the polarization potential ($E_{cathode}$) rapidly decreased from 1.1 V to a relative steady value of 0.9 V. Because of the slight change of the R_Ω, and the overpotential (η) was directly related to the $E_{cathode}$ [21,27], so it was concluded that the η was reduced from 0.47 V to 0.33 V with current passage for 240 min. After adding air flow of 100 mL min^{-1}, the initial impedance spectrum had similar trend, while the $E_{cathode}$ and η were slightly increased. Because the R_E, η and $E_{cathode}$ were related to the activation and O_2 reduction of the cathodic current/polarization on the initial LSM electrode performance [21,28], the electrochemical activation of LSM cathode may be improved with air partial pressure added. The similar results were also obtained by other researchers who found the promoting effect of the air flow on Cr deposition [26].

When the initial stage of cathode polarization had completed, the effect of Cr poison became dominant in cathode electrochemical performance. After undergoing from the current passage at 400 mA cm^{-2} and 750 °C for 1200 min, the continuous increase of R_E, $E_{cathode}$ and η were observed as shown in Fig. 6(a). The $E_{cathode}$ was 2.20 V after 1200 min, which was several times higher than the initial $E_{cathode}$ of 0.89 V. The η was obtained from 0.33 V to 1.58 V while the R_Ω remained almost constant. Similarly, the R_E increased

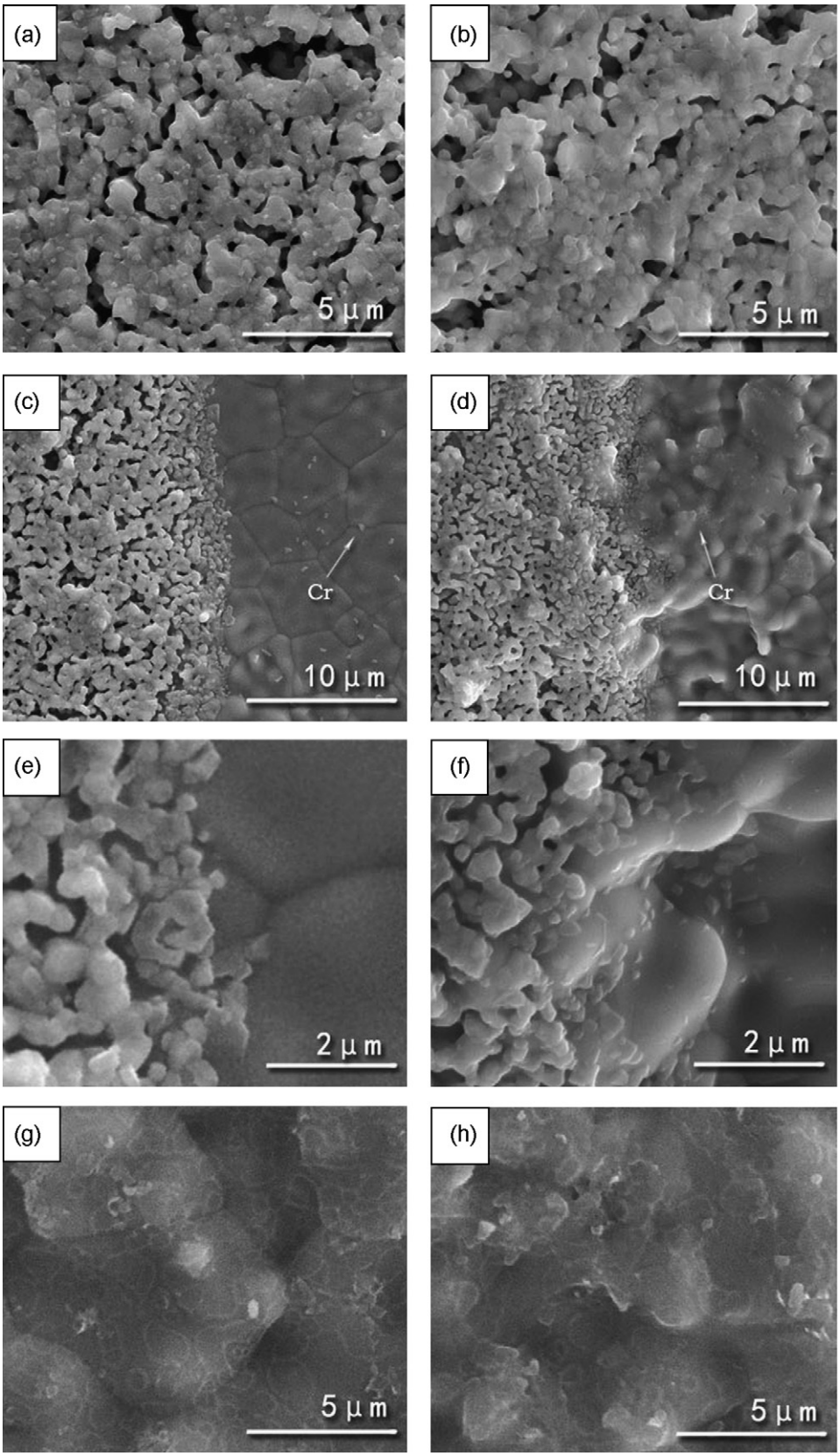

Fig. 4. SEM micrographs of the Cr deposition on the cathode in open air (a, c, e, and g) and with air flow of 100 mL min^{-1} (b, d, f, and h) at 750 °C for 1200 min: (a and b) LSM surface; (c and d) the edge of cathode; (e and f) the detail of the edge of cathode; (g and h) the surface of YSZ under cathode, the cathode was removed by HCl.

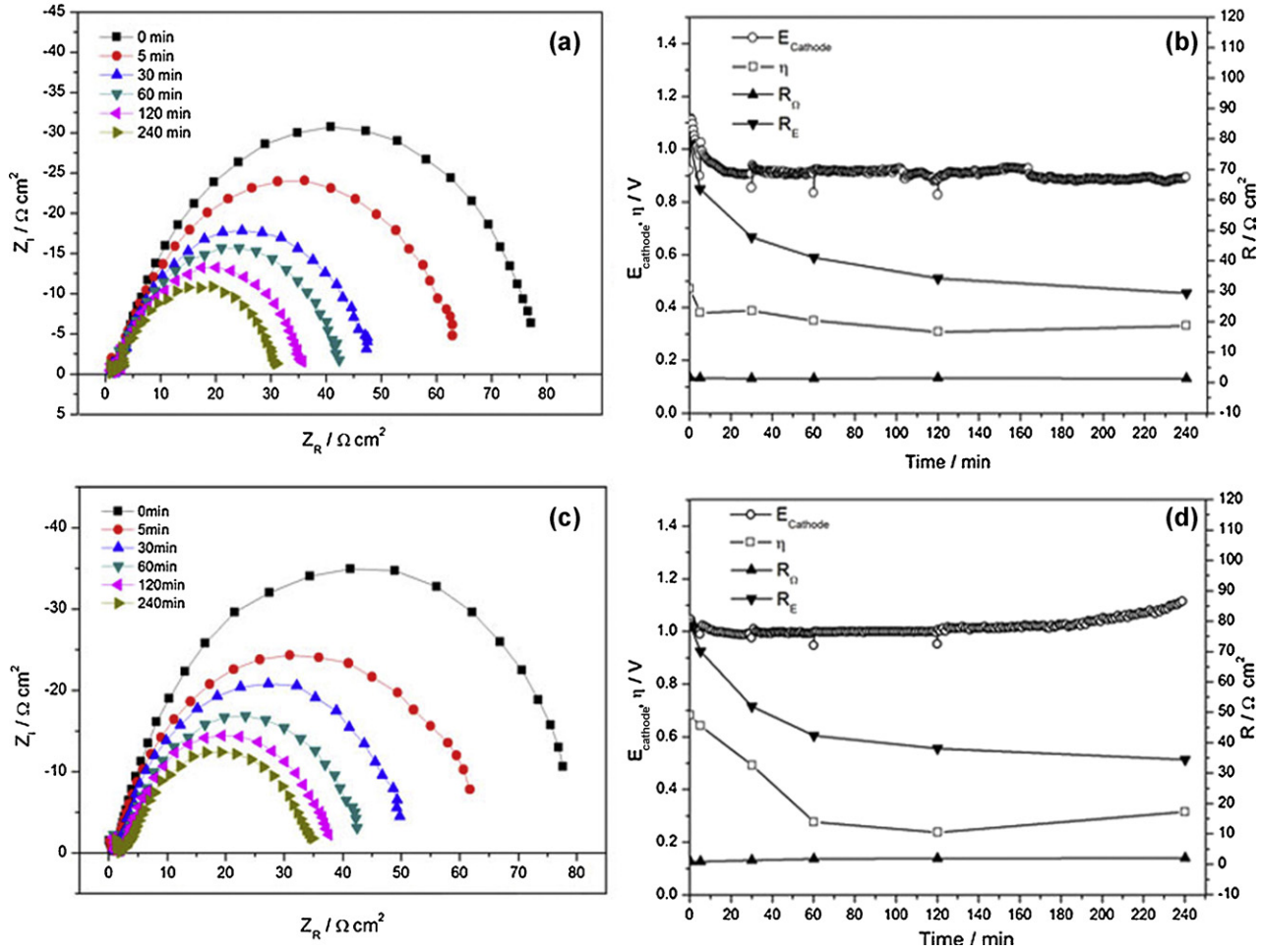

Fig. 5. Initial impedance and polarization curves of LSM cathode in the presence of Fe–Cr alloy as a function of time in open air (a and b) and with an air flow of 100 mL min^{-1} (c and d) at 750 °C with a current of 400 mA cm^{-2}.

from 29.3 Ω cm^2 to 138.7 Ω cm^2. With the air flow of 100 mL min^{-1} on the cathode side, the polarization behavior of the cathode was characterized by two distinct regions as shown in Fig. 6(b). The $E_{cathode}$ increased rapidly from 0.99 V to 2.60 V between 240 min and 400 min, and maintained relative stability for the rest of the time. This was the typical characteristic of LSM cathode polarization behavior which resulted from the O_2 reduction in the presence of Fe–Cr alloy with current passage [29,30]. The significant increases of the R_E and η imply that the Cr poison has an important influence on the O_2 reduction reaction of LSM cathode, and the kinetic process can be accelerated at the presence of air flow.

After the cathode polarization for 1200 min, the LSM cathode was found to be delaminated from the YSZ electrolyte substrate, which was in accordance with the recent researches. Yamashita et al. [31] studied the polarization behavior of LSM electrode with anodic current treatment of 300 mA cm^{-2} at 1000 °C, and found that

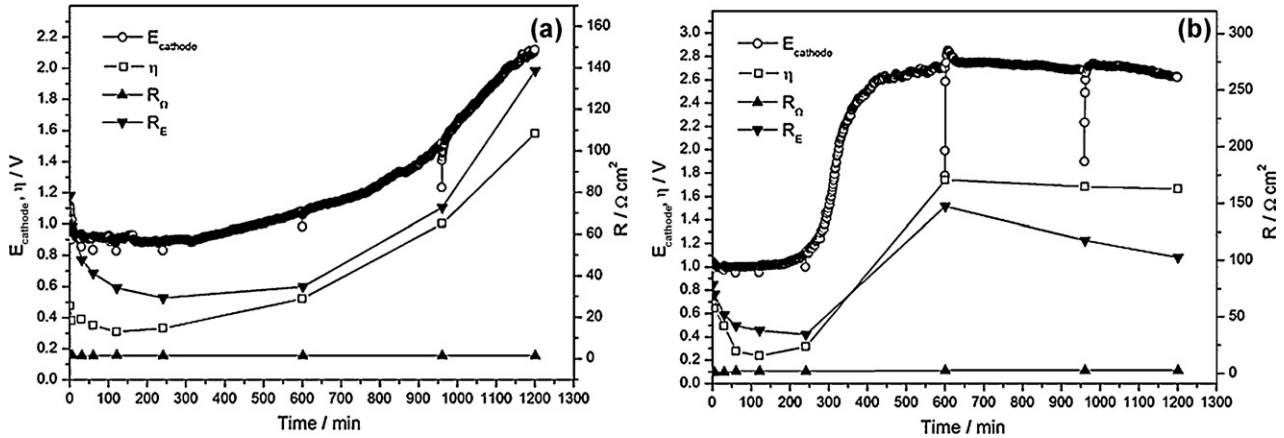

Fig. 6. Polarization curves of LSM cathode in the presence of Fe–Cr alloy as a function of time at 400 mA cm^{-2} and 750 °C for 1200 min in open air (a) and with an air flow of 100 mL min^{-1} (b).

the LSM electrode delaminated after current treatment for 600 min, accompanying with the quick increase of the polarization potential of the LSM electrode for the O_2 oxidation reaction. Jiang et al. [20] also found that the LSM electrode was completely delaminated from the TZ3Y electrolyte after cathode polarization for 360 min with current passage of 200 mA cm^{-2} at 900 °C in the presence of Fe–Cr alloy. The essence of this phenomenon can be explained by that since LSM is a predominantly electronic conductor, O_2 reduction reaction will be enhanced at the three phase boundary (TPB) region. The reaction can weaken the bondage between the cathode and electrolyte layer since Cr deposition in TPB, so the electrode layer can be delaminated from the TZ3Y electrolyte [20]. In contrast to these researchers' works, we used reduce operation temperature at 750 °C, hence the TPB area would be further reduced due to decreasing the ionic conductivity of electrode materials. Since the oxygen reduction reaction could be restricted to the TPB region, the Cr would be selectively deposited at the LSM/YSZ interface region. The growth of Cr crystal would result in the volume expansion and gradually separate LSM and YSZ layer, eventually lead to the LSM electrode delaminated from YSZ electrolyte layer.

Fig. 7 shows the SEM micrographs of the Cr deposition on the cathode after current passage of 400 mA cm^{-2} at 750 °C for 1200 min. As the cathode had partially delaminated from YSZ electrolyte, some distinctive grains were found on the exposed surface of YSZ in Fig. 7(a). When air flow was introduced, the cathode had been delaminated from the YSZ electrolyte in a larger region, and a lot of different size cubic crystals distributed on the electrolyte surface in Fig. 7(b). Meantime, there was significant Cr deposition on the edge of LSM cathode/YSZ electrolyte as shown in Fig. 7(c) and (d). The shape of the grains appeared a shape of hexagonal prism. After the cathode was totally removed by HCl solution, no tiny grain existed on the YSZ surface was observed in Fig. 7(e). However, larger cubic grains remained on the sample that was in air flow as shown in Fig. 7(f). This can be reasonably explained by the polarization behavior of LSM cathode at the presence of Fe–Cr alloy, in which Cr deposition blocks the gas diffusion and causes the delaminating of cathode layer.

Fig. 8 shows the polarization curve of LSM cathode under current passage of 400 mA cm^{-2} for 3000 min at the presence of Fe–Cr alloy. There were two obviously rapid increases in the polarization curve.

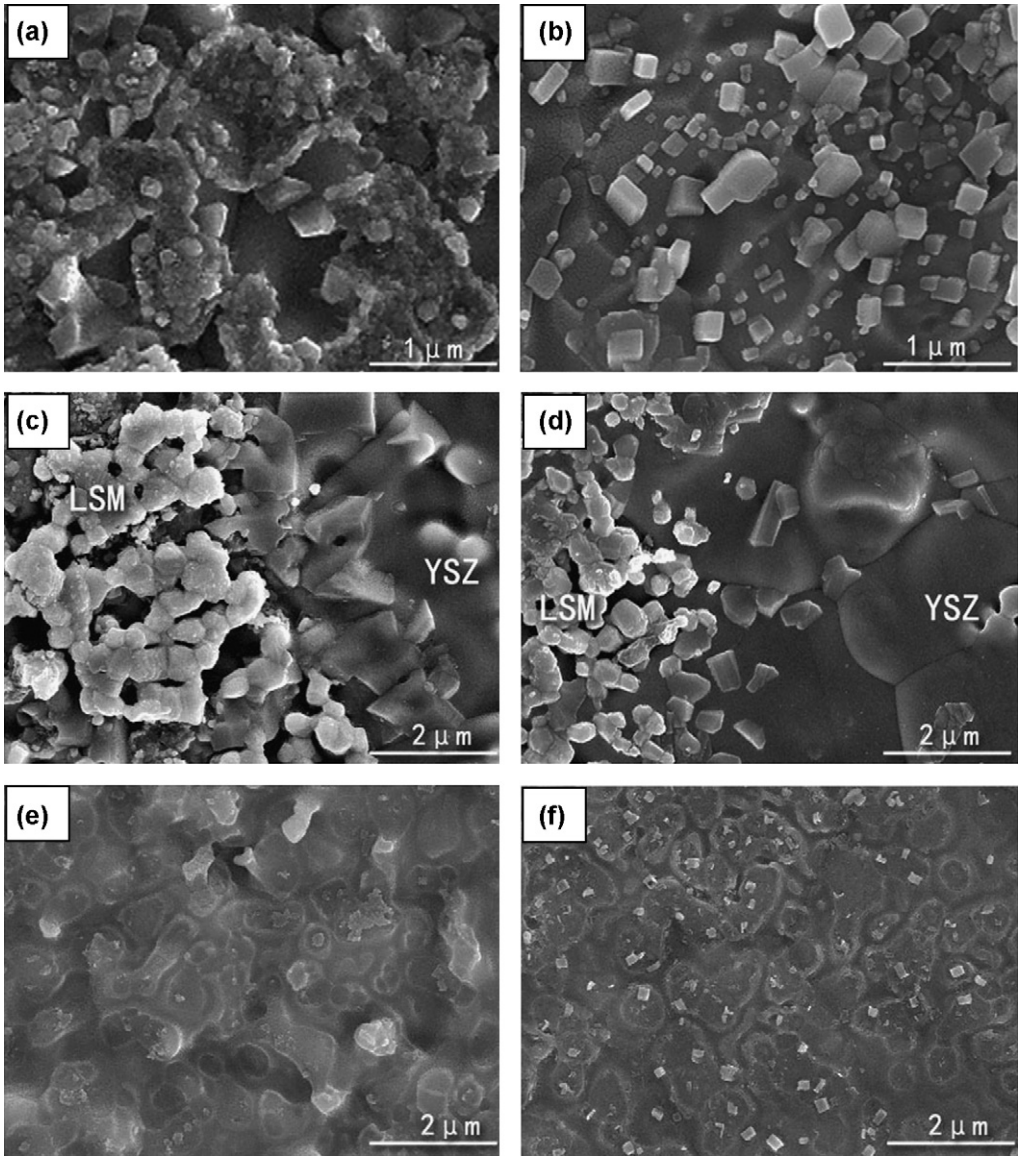

Fig. 7. SEM micrographs of the Cr deposition on the cathode in open air (a, c, and e) and with an air flow of 100 mL min^{-1} (b, d, and f) at 400 mA cm^{-2} and 750 °C for 1200 min: (a and b) LSM surface; (c and d) the edge of cathode; (e and f) the surface of YSZ under cathode, the cathode was removed by HCl.

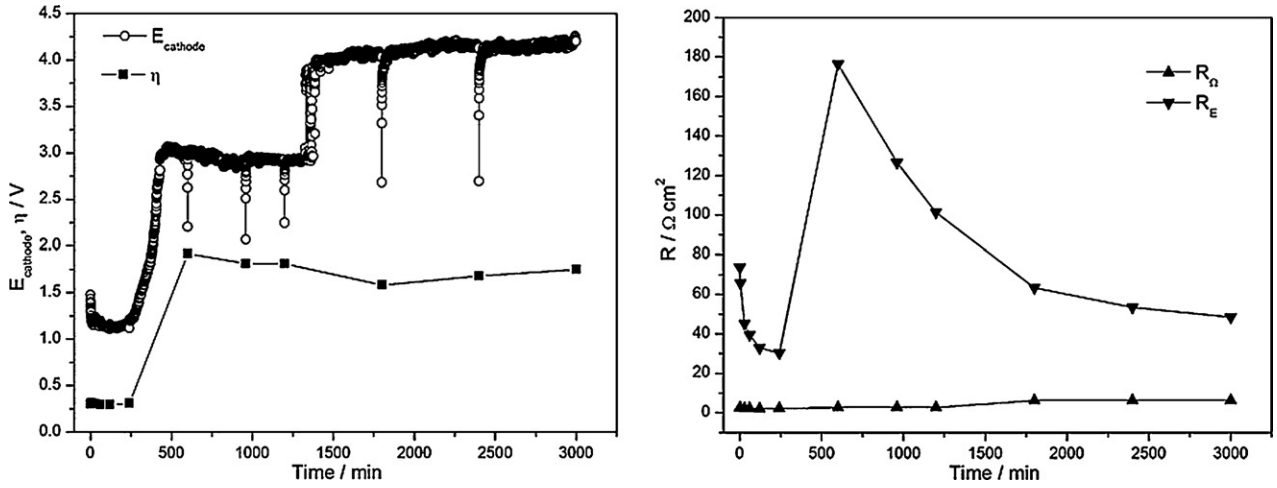

Fig. 8. Polarization curves of LSM cathode in the presence of Fe–Cr alloy as a function of time at 400 mA cm^{-2} and 750 °C for 3000 min with air flow of 100 mL min^{-1}.

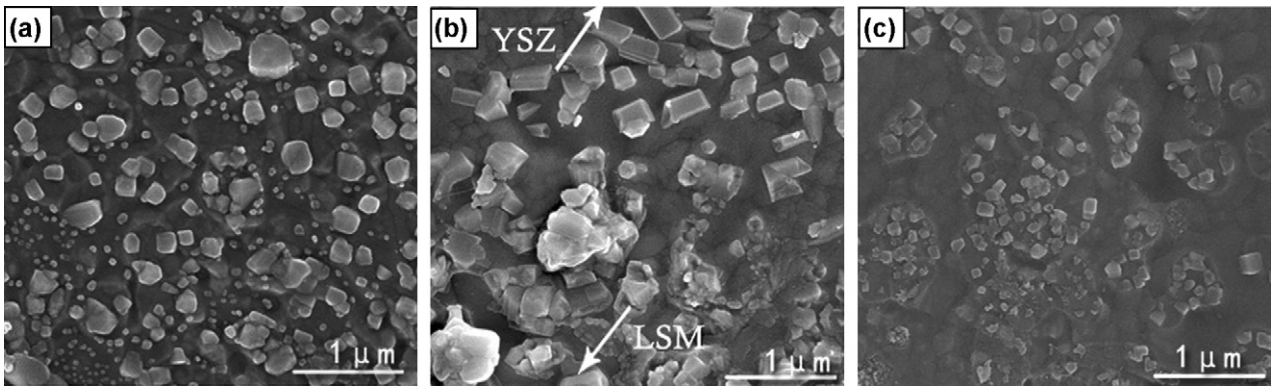

Fig. 9. SEM micrographs of the Cr deposition on the cathode with an air flow of 100 mL min^{-1} at 400 mA cm^{-2} and 750 °C for 3000 min: (a) the surface of YSZ; (b) the edge of cathode; (c) the surface of YSZ under cathode washed by HCl.

In the first rise, the polarization potential $E_{cathode}$ rapidly increased from initial 1.19 V to 2.95 V between 240 min and 540 min, then reaching a potential plateau, in which R_E increased from 32.8 Ω cm^2 to 176.0 Ω cm^2 corresponding to the change of $E_{cathode}$ as shown in Fig. 8(b). This indicates that the increase in $E_{cathode}$ is mainly due to the increases of R_E and η, as the R_Ω remains nearly constant. The essential increase in $E_{cathode}$ has been demonstrated as above which was caused by the delaminating of cathode layer. In the second rise, the $E_{cathode}$ rapidly increased from initial 2.94 V to 3.95 V after 1380 min, then increased slowly to 4.20 V for rest of the polarization time. Different to that of first region, the R_E was gradually reduced to 48.1 Ω cm^2 from 540 min to 3000 min while the R_Ω began to increase from 540 min, which indicated that the increase of R_Ω was the main reason for increase of $E_{cathode}$. Similar trend as R_E was also

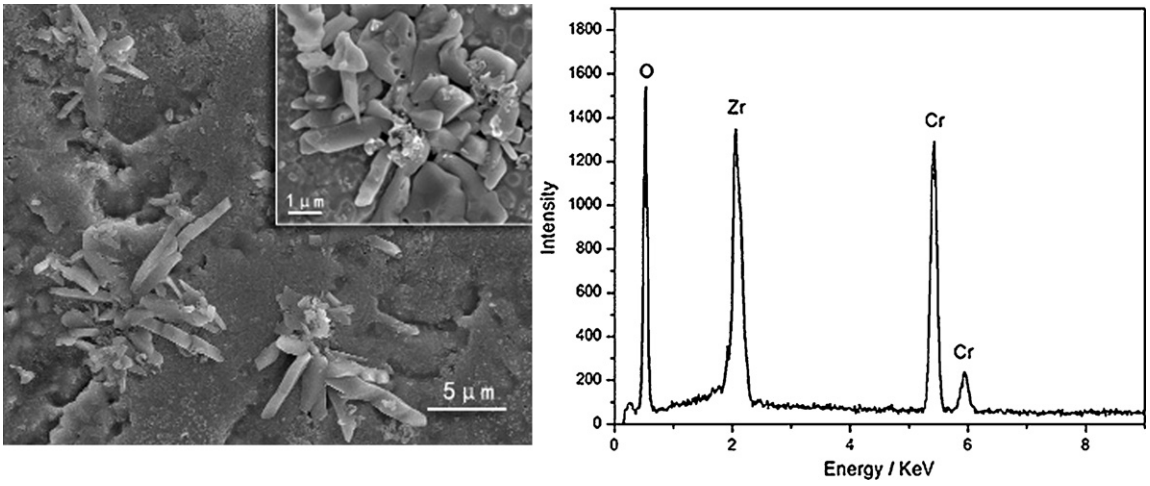

Fig. 10. EDS patterns of the deposited pieces with a divergent structure on the LSM electrode surface.

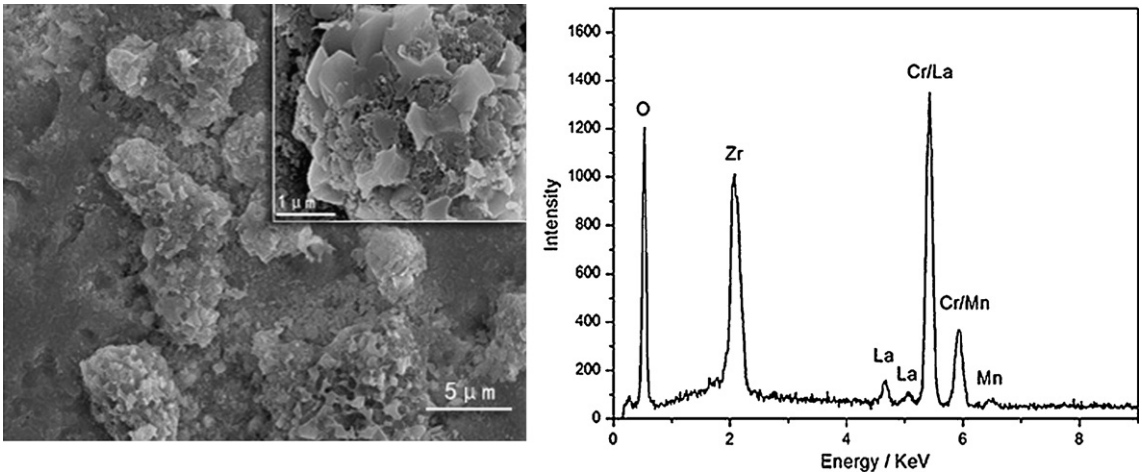

Fig. 11. EDS patterns of the deposited pieces with a ball structure on the LSM electrode surface.

observed in η. With the polarization time increase, the deposition and growth of Cr crystals would accelerate the formation of gaps between the LSM and YSZ, resulting in the irreversible performance deterioration of the cathode. So the rapid increase in $E_{cathode}$ is most likely related to the formation of a mass of Cr deposition, which inhibits the electron transport in cathode layer [20,21].

Fig. 9 shows the SEM micrographs of Cr deposition on the surface of LSM/YSZ at 400 mA cm^{-2} and 750 °C for 3000 min in an air flow of 100 mL min^{-1}. With the increase of polarization time, the cathode was further delaminated under current polarization. Fine grains were observed on the surface of YSZ electrolyte as shown in Fig. 9(a) and at the edge of cathode as shown in Fig. 9(b). The average size of Cr sediments on the surface of YSZ electrolyte was ranged from 0.1 to 0.3 μm, which is smaller than that of Cr sediments on the edge of cathode which was in the range of 0.3–0.5 μm, indicating that the Cr deposition would preferentially occur at the cathode/electrolyte interface. Fig. 9(c) shows Cr deposition rings with diameters of 0.5–1 μm and fine grains on the YSZ electrolyte surface.

There were some congregated Cr depositions with sizes of 3–5 μm found near the edge of cathode after cathode was totally removed by HCl treatment. This is probably due to the influence of air flow on the orientation formation and growth of Cr sediments. Fig. 10 shows Cr sediments with a divergent structure consisted of several strips, which were detected by the EDS analysis, indicating the formation of Cr_2O_3 oxides. The other one looked like ball structure consisted of many fine particles as shown in Fig. 11 which both Cr and Mn were detected by the EDS analysis, indicating the formation of $(Cr,Mn)_3O_4$ spinel oxides. The TPB region of LSM cathode/YSZ electrolyte has a distinctive contribution to congregate Cr sediment and form crystalline configuration under air flow and current passage.

4. Conclusion

The Cr deposition between Fe–Cr alloy interconnect and LSM cathode has been investigated at 750 °C. Generally, the Cr deposition reaction can be accelerated under air flow, and preferentially occurs on the boundary of LSM/YSZ. The Cr deposition will cause the LSM cathode layer delaminated from YSZ electrolyte, and then induce significant degradation in cathode performance. The rapid magnitude increase of $E_{cathode}$ was observed on two stages with current passage on the LSM cathode for 3000 min, which could be reasonably explained by two kinds of mechanism of cathode delaminating from electrolyte layer and a mass of Cr deposition presence. When the LSM cathode was removed from the YSZ electrolyte, the Cr deposition rings with diameters of 0.5–1 μm could be clearly observed. Two congregated Cr depositions with size of 3–5 μm were also found near the edge of cathode. One divergent structure consisting of several strips was Cr_2O_3 oxides, and the other one ball like structure consisting of many fine particles was likely to be $(Cr,Mn)_3O_4$ oxides. The orientation formation and growth of Cr sediments on the interface of LSM/YSZ is mostly due to the mechanism in three phase boundary and the effect of air flow.

Acknowledgments

This research was financially supported by the National Science Foundation of China under the project contract U1134001 and the“863” high-tech project under contract 2011AA050702. SEM and XRD analysis were assisted by the Analytical and Testing Center of Huazhong University of Science and Technology. The authors would like to thank Prof. San Ping Jiang of Curtin University for helpful discussions on the mechanism and kinetics of Cr poisoning SOFC cathode.

References

[1] P. Singh, N.Q. Minh, Int. J. Appl. Ceram. Technol. 1 (2004) 5–15.
[2] B. Hua, J. Pu, J.F. Zhang, F.S. Lu, B. Chi, L. Jian, J. Electrochem. Soc. 156 (2009) B93–B98.
[3] J.W. Fergus, Mater. Sci. Eng. A 397 (2005) 271–283.
[4] S.P.S. Badwal, Solid State Ionics 25 (2001) 16–21.
[5] J. Li, J. Pu, B. Hua, G.Y. Xie, J. Power Sources 159 (2006) 641–645.
[6] Z.G. Yang, Int. Mater. Rev. 53 (2008) 39–54.
[7] Z. Lu, J. Zhu, J. Am. Ceram. Soc. 88 (2005) 1050–1053.
[8] J. Pu, J. Li, B. Hua, G.Y. Xie, J. Power Sources 158 (2006) 354–360.
[9] H. Tu, U. Stimming, J. Power Sources 127 (2004) 284–293.
[10] F.L. Liang, J. Chen, S.P. Jiang, B. Chi, J. Pu, L. Jian, Electrochem. Solid State Lett. 11 (2008) B213–B216.
[11] B. Hua, F.S. Lu, J.F. Zhang, Y.H. Kong, J. Pu, B. Chi, L. Jian, J. Electrochem. Soc. 156 (2009) B1261–B1266.
[12] E. Konycheva, H. Penkalla, E. Wessel, U. Seeling, L. Singheiser, K. Hilpert, J. Electrochem Soc. 153 (2006) A765–A773.
[13] C. Gindorf, L. Singheiser, K. Hilpert, Steel Res. 72 (2001) 528–533.
[14] N. Dishovskid, A. Petkova, I. Nedkov, I. Razkazov, IEEE Trans. Magn. 30 (1994) 969–971.
[15] H.S. Cho, S.S. Kim, IEEE Trans. Magn. 35 (1999) 3151–3153.
[16] S. Taniguchi, M. Kadowaki, H. Kawamura, T. Yasuo, Y. Akiyama, Y. Miyake, T. Saitoh, J. Power Sources 55 (1995) 73–79.
[17] K. Fujita, K. Ogasawara, Y. Matsuzaki, T. Sakurai, J. Power Sources 131 (2004) 261–269.
[18] S.P.S. Badwal, R. Deller, K. Foger, Y. Ramprakash, J.P. Zhang, Solid State Ionics 99 (1997) 297–310.
[19] K. Fujita, T. Hashimoto, K. Ogasawara, H. Kameda, Y. Matsuzaki, T. Sakurai, J. Power Sources 131 (2004) 270–277.
[20] S.P. Jiang, J.P. Zhang, L. Apateanu, K. Foger, J. Electrochem. Soc. 147 (2000) 4013–4022.
[21] S.P. Jiang, J.P. Zhang, X.G. Zheng, J. Eur. Ceram. Soc. 22 (2002) 361–373.

[22] Y.D. Zhen, L. Jian, S.P. Jiang, J. Power Sources 162 (2006) 1043–1052.
[23] C.J. Fu, K.N. Sun, X.B. Chen, N.Q. Zhang, D.R. Zhou, Electrochim. Acta 54 (2009) 7305–7312.
[24] Y.D. Zhen, S.P. Jiang, J. Power Sources 180 (2008) 695–703.
[25] S.P. Jiang, Y.D. Zhen, S. Zhang, J. Electrochem. Soc. 153 (2006) A1511–A1517.
[26] C. Gindorf, L. Singheiser, K. Hilpert, J. Phys. Chem. Solids 66 (2005) 384–387.
[27] Y.D. Zhen, A.I.Y. Tok, S.P. Jiang, F.Y.C. Boey, J. Power Sources 170 (2007) 61–66.
[28] S.P. Jiang, J. Solid State Electrochem. 11 (2006) 93–102.
[29] X.B. Chen, L. Zhang, S.P. Jiang, J. Electrochem. Soc. 155 (2008) B1093–B1101.
[30] X.B. Chen, B. Hua, J. Pu, J. Li, L. Zhang, S.P. Jiang, Int. J. Hydrogen Energy 34 (14) (2009) 5737–5748.
[31] Yamashita, H. Tsukuda, T. Hashimoto, Proceedings of the 1st European Solid Oxide Fuel Cells Forum, European Fuel Cell Group, Lucerne, Switzerland, 1994, p. 661.